DOI: 10.2478/ace-2013-0025

A NEW HIGH-EFFICIENCY PROCEDURE FOR AGGREGATE GRADATION DETERMINATION OF THE RAILWAY BALLAST BY MEANS IMAGE RECOGNITION METHOD

M. GUERRIERI[1], G. PARLA[2]

The mechanical characteristics of the railway superstructure are related to the properties of the ballast, and especially to the particle size distribution of its grains. Under the constant stress-strain of carriages, the ballast can deteriorate over time, and consequently it should properly be monitored for safety reasons. The equipment which currently monitors the railway superstructure (like the Italian diagnostic train Archimede) do not make any "quantitative" evaluation of the ballast. The aim of this paper is therefore to propose a new methodology for extracting railway ballast particle size distribution by means of the image processing technique. The procedure has been tested on a regularly operating Italian railway line and the results have been compared with those obtained from laboratory experiments, thus assessing how effective is the methodology which could potentially be implemented also in diagnostic trains in the near future.

Keywords: Railway ballast, Image analysis, Segmentation techniques, Aggregate gradation.

1. Introduction

Ballast is defined as granular material of specified properties placed on the formation to provide vertical and lateral support to the sleepers. Ballast layer maintain an adequate stability to the sleepers against vertical, lateral and longitudinal forces generated by rolling stocks. Also, ballast layer provides adequate dynamic resilience for the railway track and provides sufficient permeability for drainage.

In order to guarantee high security levels for users and effectively manage railway maintenance activities, high efficiency techniques have been employed to monitor the railway superstructure, like those implemented in the so-called diagnostic trains (e.g. "the Archimede train"). However, this equipment does not currently allow to evaluate any quantitative degradation of the ballast, and especially its particle size distribution. A specific research has therefore been carried out to develop a procedure for determining

[1] University of Enna "Kore" and Adjunct Professor at University of Palermo, Italy, Via della Cooperazione, Enna Bassa 94100, Enna, Italy, Tel: 39-935-536-350, e-mail: marco.guerrieri@tin.it, (Corresponding Author).

[2] DICAM, Faculty of Engineering, University of Palermo, Italy. Viale delle Scienze al Parco d'Orleans, Palermo, Italy 90128, e-mail: giuseppe.parla@unipa.it

railway ballast particle size distribution by means of the image processing technique. Such a technique has already given very good results when adopted in railway monitoring [1, 2, 3, 4, 5] as well as in numerous other fields of transport engineering [6, 7, 8, 9, 10, 11]. The equipment used in the analyses consists of a high-resolution 16.1MP camera placed on a tripod at a prefixed height of 0.80 m. The experimentation has been conducted on a new Italian railway line, along the section "*EMS/La Malfa – Cardillo*" in Palermo which already had laboratory data acquired by a certified authority and in complete conformity with the Italian Railway Network Specifications (*Capitolato RFI*, n. XXXX OD D IF SP XX.XX.X.X 001 B). The surveys have covered three distinct positions which were at a distance of 10 metres the one from the other along the same railway line, and whose granulometric curves have been extracted and properly compared with the laboratory results obtained by a body independent of the research group. The methodological procedure is described below.

2. Digital image segmentation

According to Ballard [12], the digital image segmentation is the process of subdividing an image into distinct regions that are homogeneous with respect to a certain quality (Region of Interest, ROI – in this case the stone aggregates of the railway ballast). This implementation has started by adopting Otsu's method [13] for a preliminary threshold segmentation of the image complementary to that under examination. Exactly on this image, the suggested procedure investigates areas of uncertainty which can misdefine grain boundaries. As a matter of fact, the thresholded image with Otsu's method is highly influenced by the colorimetric intensity of each grain and/or by the local lighting variations of the scene which, on the other hand, in outdoor environment, are highly dependent of the time when the image is taken. In light of the above, the suggested procedure extracts the grain boundaries from the original image by means of the iterative algorithm discussed in [1, 2, 3]. Once closed and connected regions of grains have been obtained, their boundaries have been processed via a specifically adapted Watershed-type algorithm [13, 14] in order to check and, if needed, repair the irregularities in the grain boundary shape as well as to subdivide the connected regions with a slight difference in colorimetric texture. In the final part, the procedure extracts the quantities of interest to determine the aggregate particle size distribution [5] under examination.

3. Threshold segmentation, digital image binarization

Considering the contrast between grains and image background, it is possible to proceed with threshold image segmentation in order to classify and distinguish the pixels into homogeneous classes, based on their intensity variance. By accurately analysing the image fragment shown in Figure 2, the real spatial position of crushed stone grains is

seen to create some darker areas as a result of the grain neighbourhood and their mutual contact positions.

This procedure investigates these parts in order to adjust any irregularity in the separation areas between two adjacent grains. Figure 3 illustrates the complement image [13, 14, 15] in order to emphasize the darkest areas via higher light intensities.

By assuming a unique and arbitrary threshold value, the image is divided into different regions with closed and connected boundaries. Each region comprises only one pixel whose intensity is lesser or higher than the threshold value. By modifying the threshold value, also the shape and/or the number of the image-segmented regions change. The image can also be segmented by arbitrarily setting different threshold values. In order to fix the number of the thresholds and their respective values, it is advisable to analyze the shape of the pixel intensity histogram. For instance, in the image of Figure 3 the application of Otsu's method develops the binary image as in Figure 4 and its respective pixel intensity (variance) histogram is illustrated in Figure 5.

Fig. 1. Front view of camera and tripod

Fig. 2. Image fragment related to the first position

Fig. 3. Image complement of Fig. 2

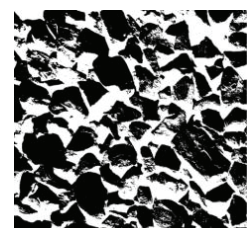

Fig. 4. Otsu's method on the complement image shown in Figure 2

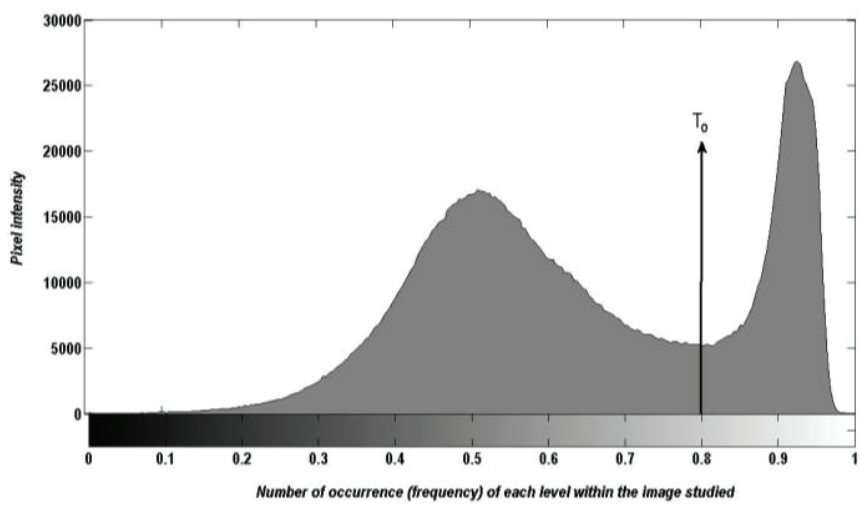

Fig. 5. Otsu's method on the image

Furthermore, it has been ascertained that [1, 2, 3], though individually segmented, each chromatic plane (RGB) of the same image provides, as expected, results that are almost identical. In order to simplify and to speed up the whole procedure, only the red chromatic plane was subject to thresholding. The image downstream of the previous threshold elaborations is shown in Figure 4. It is however worth noting that the binary image with a unique threshold obtained after segmentation (via Otsu's or any other method) is affected by evident irregularities due to the following reasons:

– some regions, though visually separated, are not divided because of their mutual position;
– the colorimetric texture of (micro or macro) cracks in the same grain sometimes leads to a non-realistic subdivision of the grain itself;
– the boundaries given by thresholding are different from those obtained via the Watershed method and certainly more reliable.

In order to eliminate or reduce the irregularities listed above, appropriate morphological boundary operators [14, 15, 16, 17] have been used to detect and close small white cracks within each grain surface, which appear black in the thresholded image shown in Figure 4. The result is given in Figures 6 and 7. It is moreover worth observing that for expository reasons Figure 6 shows the grain cavities of the complement image which are depicted green in Figure 4, while the image in Figure 7 displays the final result.

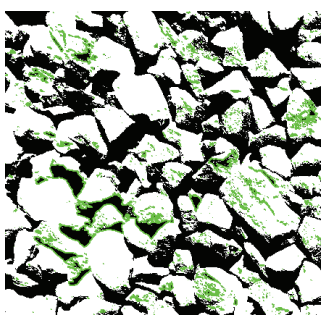

Fig. 6. Grain coarseness

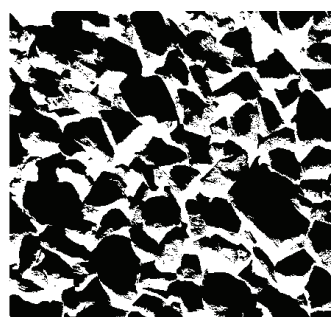

Fig. 7. inal outcome after closing grain coarseness

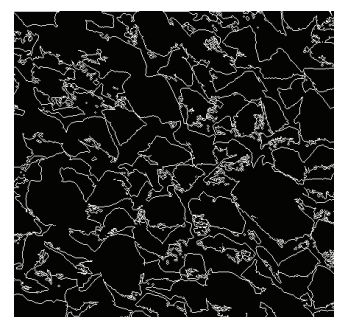

Fig. 8. Boundaries

The next step is to extract the boundary contours {C} between grains from the image in Figure 7 and there marked in black. To this end, an appropriate binary morphological function [1, 2, 14, 16] encodes every grain perimeter which, in this image, also represents the possible separation surface from the background. The result of such an activity is reported in Figure 8. Next, the suggested methodology investigates the transition areas between a grain and the darkest background regions with regard to every edge of the points detected in domain {C}.Indeed, the uncertainty about defining the grain boundary is highly dependent on how effectively any pixel which

belongs to the grain and to the background at the same time, is eliminated (areas of uncertainty). In light of what just said and reported in [1, 2, 3, 4, 5, 6], it follows as such: Let us consider, for clarity reasons, a part "A" of the image of Figure 2 shown in Figure 9.

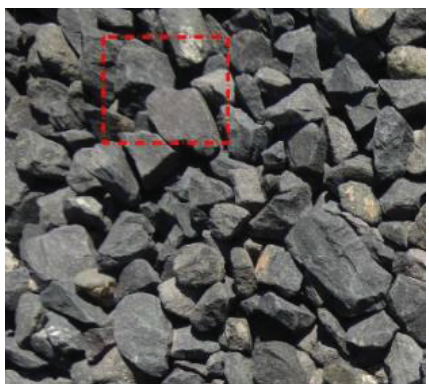

Fig. 9. Ballast image

Fig. 10. Zoom of the ballast image

A median filter is applied through the following relation:

(3.1) $$M = A * B$$

where in this specific case the template B has a definite [3X3] dimension and a coefficient equal to (1/9).

(3.2) $$B = \left(\frac{1}{9}\right) * \begin{bmatrix} 1 & 1 & 1 \\ 1 & 1 & 1 \\ 1 & 1 & 1 \end{bmatrix}$$

The relation (1) can be interpreted as a 3x3-sized window moving on the image, from one pixel to another, both on the rows and the columns. Within this window the products are computed by multiplying the image intensity levels and the corresponding values of the filter which is, in this case, developed as the mean of the eight adjacent pixel values. The resulting value replaces, each time, the central pixel of the template B on the image A. Typically, by a two-dimensional signal, like a digital image, a median filter (1) tends to eliminate the noise (high-frequency disturbance), but simultaneously it introduces an image blurring effect to mitigate the steps constituting the details of the filtered objects (coarse boundaries, etc.).

It follows that the ideal would be to find the optimum compromise between noise removal and detail preservation. This procedure iteratively applies the previous

filter so as to spread the numerical values of all the pixels which certainly belong to a colorimetrically homogeneous area, be it the grain or the background. It results that the image at time "t" (iteration step) derives from the original image convolved with the median filter (1), or:

$$A(i,j,t) = A_0(i,j) \times M(i,j,t) \tag{3.3}$$

where (i,j) are the pixel position indices within the original matrix A and × stands for the convolution operator. For congruence reasons, it is necessary to attribute every generic pixel occupying the position [i, j] to a colorimetrically homogeneous area (be it the grain or the background), so as not to eliminate the fundamental information of their boundaries. Moreover, since the expanded mean filter (3) tends to remove the information on the edge details, this effect should be mitigated by applying another operator which, instead, emphasizes grain boundaries. In light of the above, downstream of the previous convolution (3), an edge extraction operator labelled range operator [14, 15], has necessarily been applied. This non convolutive filter type allows to replace the central pixel with the range difference of the template B selecting the chromatic intensities of image A, which has a [3x3] size as well. For each deviation (i,j) from the template B, the value of the central pixel can therefore be formalized as follows:

$$\begin{aligned} \mathrm{R(i,j)} = (&\mathrm{MAX}(\mathrm{A_{i-1,j-1}; A_{i-1,j}; A_{i-1;j+1}; A_{i,j-1;}A_{i,j}; A_{i,j+1}; \ldots; A_{i+1,j+1}})\text{-} \\ &\mathrm{MIN}(\mathrm{A_{i-1,j-1}; A_{i-1,j}; A_{i-1;j+1}; A_{i,j-1;}A_{i,j}; A_{i,j+1}; \ldots; A_{i+1,j+1}})); \end{aligned} \tag{3.4}$$

So, the range values of every [3X3] boundary of all the pixels belonging to the original image A have been sought and highlighted. Such a filter allows to define some chromatic intensity values which will fill a matrix having information on element contours. These values are then subtracted from matrix M, thus reducing the pixel intensities which mark the boundary of every grain. The result of such an iterative process is illustrated in Figure 11.

$$\mathrm{J(i,j,t)} = \mathrm{J(i,j)} + \mathrm{abs(M(i,j,t) - R(i,j,t))}, \tag{3.5}$$

As a matter of fact, by examining every pixel intensity profile (Figure 12) corresponding to any direction between the grain boundary and the background area (represented by the red line in Figure 11), it results that while the relation (1) tends to make numerically uniform the pixel value on the point edge under consideration, the relation (4) on the same contour lowers the values in the darkest areas and therefore colorimetrically near the background. In other words, the aim has been to modify the numerical pixel values of the ballast grains on the external as well as the internal regions in order to make them as colorimetrically uniform as possible.

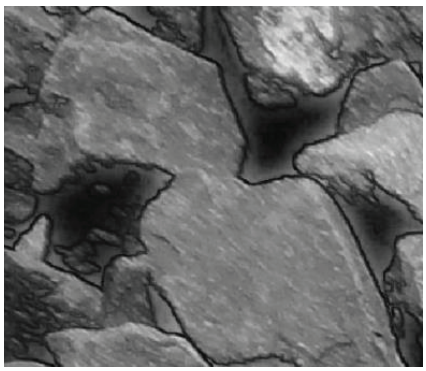

Fig. 11. Application of the iterative process of Equation 5

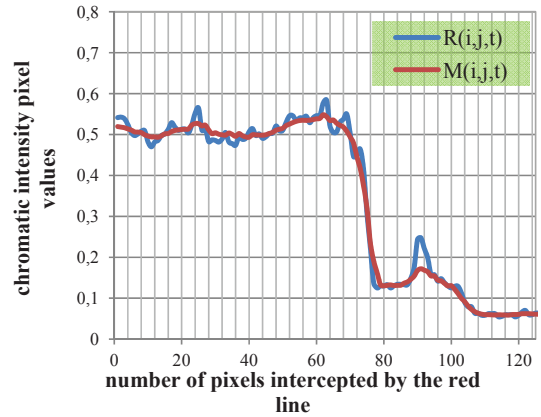

Fig. 12. Comparison between pixel intensity profiles

4. Image segmentation with the Watershed transform

Once determined the Boolean matrix of Figure 14 by means of the Equation 10, the same image has been processed by the Watershed method. Such a methodology allows to segment an image by interpreting the pixel values as "parts" with respect to a preset reference value.

Moreover the Watershed algorithm has been applied for better analyzing the shape of closed and connected regions previously obtained and for their eventual correction. With regard to the implemented algorithm, all the points near the grain boundaries and in their internal regions adequately modified have been considered as "significant markers" (see Figure 13).

In order to have a range of markers "correctly" displayed in a Boolean image, it has been necessary to use a morphological operator known as "Boolean distance", which attributes a progressive numerical value to every non-null pixel as a function of the distance from the closest null pixel. This way the separation lines between grains have precisely been defined and the equidistant areas have been highlighted, thus obtaining numerical information on the three-dimensional characteristics of the grain shape along the separation surface.

The final outcome of the above procedure is illustrated in Figure 14 where a superposition of the results from the Watershed application to boundaries onto the original image is shown with different colours, while in Figure 15 the grain and grain boundaries and separation surfaces downstream of the Watershed transform have been isolated.

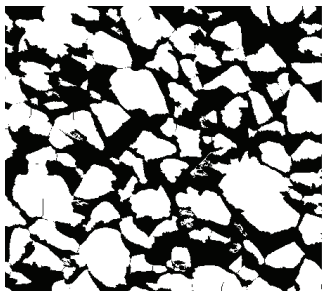

Fig. 13. Application of the congruence functions

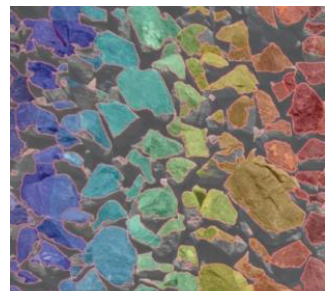

Fig. 14. Result of the Watershed algorithm application

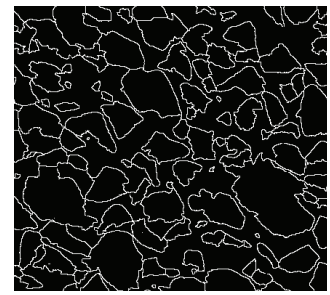

Fig. 15. The Watershed transform boundaries

5. Determination of the geometric quantities of interest

For the purpose of this research, some geometric quantities which characterize the shape of the grains previously identified have been determined. Once the boundary has been identified (see Figure 15), the following geometrical object data can easily be acquired [1, 2, 3, 16, 18, 19, 20]:

- area (A): expressed in terms of number of the pixels representing the object;
- perimeter (P): expressed in terms of number of the pixels constituting the boundary, denoted with P;
- compactness (C): given by the following ratio C=P2/A (the square of the perimeter makes the ratio independent of the real object dimensions).
- minor axis of the ellipse: centred on the barycentre of every grain and with the same normalized second-order central moment. For the aim of this research, this axis will later be assumed as coinciding with the diameter found for every single grain.
- major axis of the ellipse: centred on the barycentre of every grain and with the same normalized second-order central moment.

With regard to the image fragment of Figure 2, some of the previously discussed quantities are shown in Figure 16.

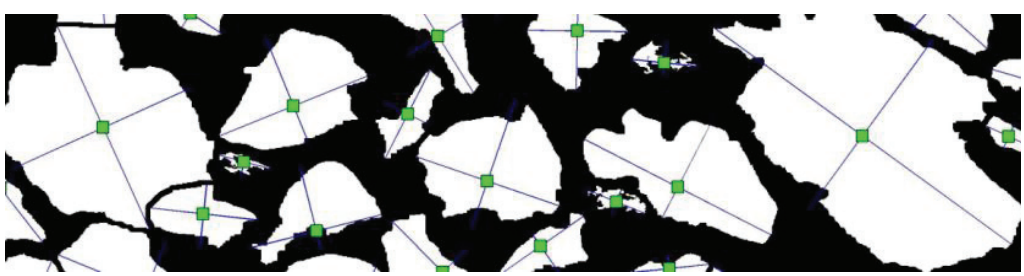

Fig. 16. Representation of the quantities of interest on the Boolean image

6. Application and results

Ballast normally is comprised of particles ranging in size from 1.18 to 63 mm, with majority of articles in the 28 to 50 mm size range. A comparison of particle sizes for British (Network Rail), German (Deutsche Bahn AG), Indian (Indian railways), Australian (Australian Rail Track Corporation) and Turkish (Turkish Railways) systems is given in Table 1 [21, 22, 23].

Table 1

Comparison of particle size distribution of ballast

British Network Rail		**German Railways**		**Indian Railways**		**Australian Rail Track**		**Turkish Railways**	
Size	Cumulative	Size	Cumulative	Size	Cumulative	Size	Cumulative	Size	Cumulative
(mm)	% Passing	(mm)	% Passing	(mm)	% Passing	(mm)	% Passing	(mm)	% Passing
63	100	63	100	65	95-100	63	100	63	97-100
50	70-100	50	65-100	40	40-60	53	85-100	50	67-100
40	30-65	40	30-65	20	0-2	37.5	20-65	40	25-68
31.5	0-25	31.5	0-25			26.5	0-20	31.5	0-28
22.4	0-3	25				19	0-5	22.4	0-5
32-50	≥ 50					13.2	0-2		
						4.75	0-1		
						0.075	0-1		

In light of what has been said so far and starting from the planar RGB image of the three observation points of the ballast under examination (railway section EMS/ La Malfa – Cardillo, Italy), the quantities of interest (area, dimension, orientation of the minimum diameter of each segmented grain) have been extracted. Afterwards these geometric quantities have been calibrated in order to convert every quantity measured in the image, expressed in pixel, into the real one. It is generally known that in an image the dimension of the same object [1, 2], set at a fixed distance from the camera, differs according to the position occupied in the image itself. These differences, due to the peculiarity of the camera optics, are systematic and may therefore be evaluated via the projective geometry or via image resampling (a comparison is made between the real dimensions of the object and those of its representation). It has then been sufficient to compare the dimensions of few grains depicted in the images with the real ones, via simple geometric proportions. For the three positions under examination the respective aggregate gradation curves are given in Figures 17 to 19, together with the granulometric curves from laboratory analyses carried out with classical sieving [24]. Noticeably, the granulometric curves obtained via the method described in this paper are virtually identical to those from the laboratory tests.

Table 2

Estimate aggregate gradations and Laboratory aggregate gradations

	Position N. 1					Position N. 2					Position N. 3				
Sieve size (mm)	**22,4**	**31,5**	**40**	**50**	**63**	**22,4**	**31,5**	**40**	**50**	**63**	**22,4**	**31,5**	**40**	**50**	**63**
Real passing sieve (%)	2,95	18,69	43,68	81,89	100	2,95	18,69	43,68	81,89	100	2,95	18,69	43,68	81,89	100
Average esti-mated passing sieve (%)	2,78	17,04	48,61	84,48	100	1,97	16,53	47,83	81,63	100	2,61	19,20	48,12	79,52	100
Δ	0,17	1,65	4,93	2,59	0	0,99	2,17	4,15	0,26	0	0,35	0,51	4,44	2,38	0

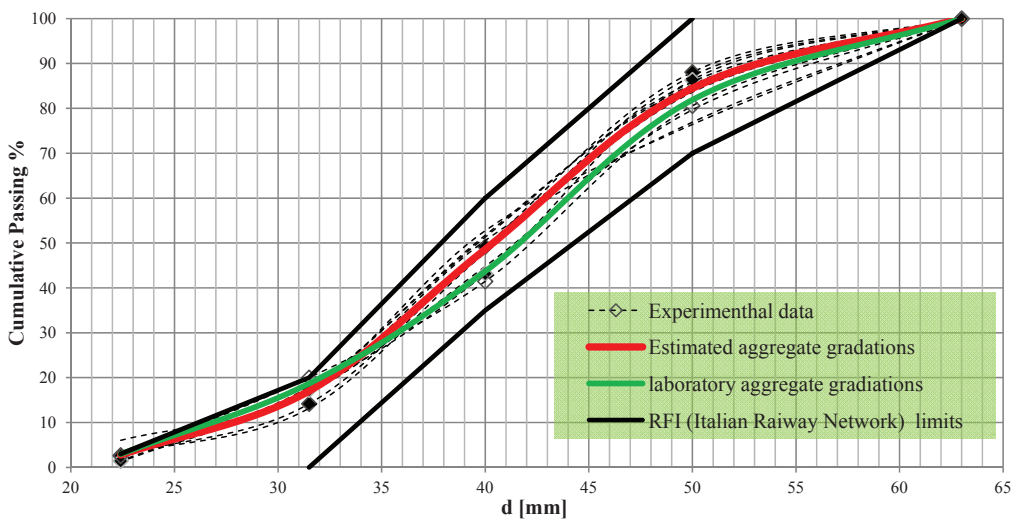

Fig. 17. Granulometric curve, Position No. 1

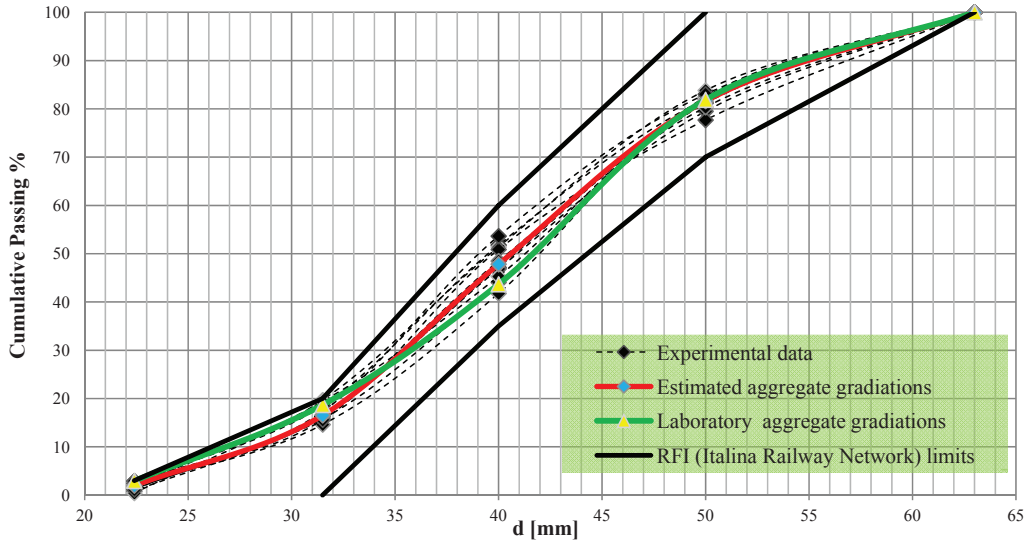

Fig. 18. Granulometric curve, Position No. 2

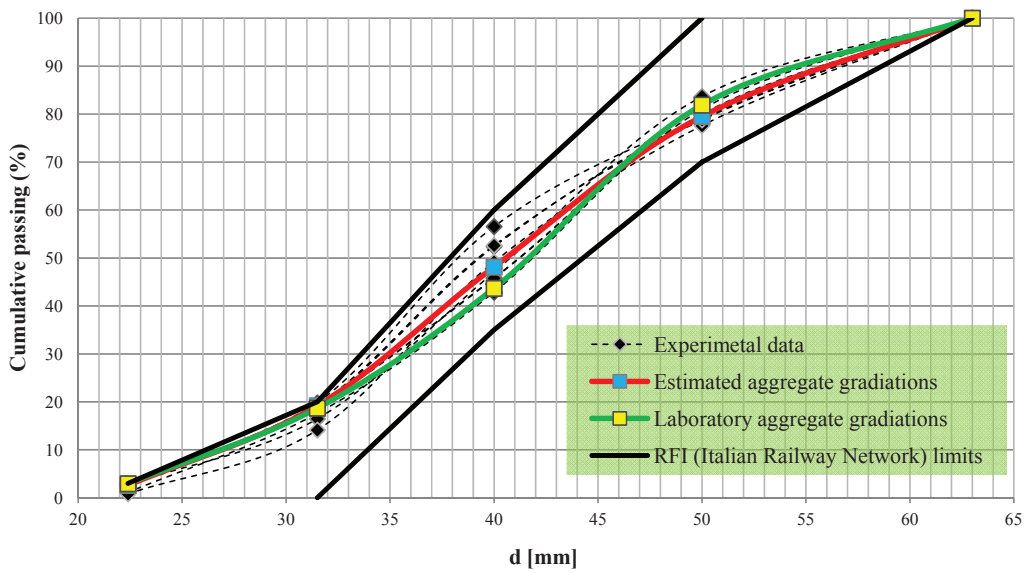

Fig. 19. Granulometric curve, Position No. 3

7. Conclusions

The aim of this research is to introduce an alternative methodology to obtain granulometric curves of the railway ballast very quickly and without any laboratory analysis. The suggested procedure, based on the image processing technique, is suitable to be complementary to the high efficiency equipment already used to monitor the superstructure. For the scope of this research, the image segmentation methods by Otsu and Watershed have been used.

The research has involved specific experiments on a regularly operating Italian railway line. On the section under examination, the aggregate gradation curves have been determined in three different major positions and they have next been compared with those obtained for the same positions through laboratory analyses, carried out by a body independent of the scholars, authors of the research. Looking at the optimum results in terms of analysis precision and speed, the methodology could be employed to carry out both field surveys on specific points of interest for the railway managing body and high efficiency surveys, and be implemented in the near future so as to improve a specific equipment for diagnostic trains, already operating in other railway networks.

Acknowledgements

The authors are grateful to Italferr S.p.A. (Palermo, Italy) for providing the Laboratory aggregate gradation analyses and to RFI S.p.A. for supplying materials and technical support.

References

1. M. Guerrieri, G. Parla, D. Ticali. Mono and stereoscopic image analysis for detecting the transverse profile of worn-out rails. *Procedia - Social and Behavioral Sciences*, ISSN: 1877-0428, Volume 53, 2012; pp. 611-621
2. M. Guerrieri, G. Parla, D. Ticali, Corriere F. Tramway Track: a New Approach for Measuring the Transverse Profile of Worn-Out Rails. *AASRI Procedia*, Volume 3, 2012; p. 451-456, ISSN: 2212-6716. Elsevier.
3. M. Guerrieri, G. Parla, D. Ticali. A theoretical and experimental approach to reconstructing the transverse profile of worn-out tracks. *Ingegneria Ferroviaria*, ISSN: 0020-0956, Vol. 67, Issue 1, 2012; pp. 23-37.
4. M. Guerrieri, D. Ticali. Sustainable mobility in park areas: the potential offered by guided transport systems. *ICSDC 2011: Integrating Sustainability Practices in the Construction Industry*, pp. 661-668, ISBN 9780784412046, ASCE Conf. Proc. doi:10.1061/41204(426)81.

5. M. Guerrieri, D. Ticali. Design standards for converting disused railway lines into greenways. *ICSDC 2011: Integrating Sustainability Practices in the Construction Industry*, p. 654-660, ISBN 9780784412046, ASCE Conf. Proc. doi:10.1061/41204(426)80
6. L. Bruno, G. Parla, C. Celauro. Image analysis for detecting aggregate gradation in asphalt mixture from planar images. *Construction and Building Materials*, Vol. 28, Issue 1, 2012; pp. 21-30. DOI:10.1016/j.conbuildmat.2011.08.007.
7. M. Guerrieri, G. Parla, F. Corriere. *A new methodology to estimate deformations of longitudinal safety barrier*. ARPN Journal of Engineering and Applied Sciences, ISSN 1819-6608, Vol. 8, N. 9, September 2013, pages 763-769.
8. M. Guerrieri, F. Corriere, G. Parla, D. Ticali. Estimation of pollutant emissions from road traffic by image processing techniques. A case study in a suburban area. *ARPN Journal of Engineering and Applied Sciences,* ISSN 1819-660, Vol. 8, n 8, 2013.
9. F. Corriere, M. Guerrieri, D. Ticali, A. Messineo. Estimation of air pollutant emissions in Flower roundabouts and in conventional roundabouts. *Archives of Civil Engineering*, LX, 2, 2013; pp. 229–246, DOI: 10.2478/ace-2013-0012.
10. F. Corriere, D. Di Vincenzo, M. Guerrieri. A logic fuzzy model for evaluation of the railway station's practice capacity in safety operating conditions. *Archives of Civil Engineering*, ISSN: 1230-2945, LIX, 1, 2013, pp.3-19, DOI: 10.2478/ace-2013-0001.
11. F. Corriere, G. Rizzo, M. Guerrieri. Estimation of air pollutant emissions in "Turbo" and in conventional roundabouts. *Applied Mechanics and Materials,* vol. 394, p. 597-604, Trans Tech Publications, Switzerland, ISBN: 978-3-03785-832-5, ISSN: 1660-9336, ISSN web 1662-7482, doi: 10.4028/www.scientific.net/AMM.394.597.
12. D.H. Ballard, C.M. Brown. *Computer Vision*, Prentice-Hall Inc., New Jersey, 1982.
13. N. Otsu. A threshold selection method from gray-level histograms. *IEEE Trans. Systems, Man, and Cybernetics*, 9(1):62-66; 1979 .
14. WK Pratt. *Digital image processing*. New York, New Jersey: John Wiley & Sons,Inc.; 2001
15. RC Gonzales, RE Woods. *Digital image processing*. 2nd ed. Upper Saddle River, New Jersey: Prentice Hall; 2002.
16. RC Gonzales, RE Woods, SL Eddins. *Digital image processing using Matlab*. Upper Saddle River, New Jersey: Prentice Hall; 2004.
17. H. Freeman. On the encoding of arbitrary geometric configurations. I*RE Trans Electron Comput.,* 1961; EC-10:260–8.
18. M. Moaveni, S. Wang, J. Hart, E. Tutumluer, N. Ahuja. Aggregate size and shape evaluation using segmentation techniques and aggregate image processing algorithms. *TRB 2013 Annual Meeting* (Accepted for Presentation and Publication at the 92nd Annual Meeting of the Transportation Research Board), Washington, DC, January 2013.
19. P. Chen, Z. Zhang, Y. Han, F. Chen, & B. Tang. Microscopic image segmentation based on iterative grid clustering. Paper presented at the *2012 19th International Conference on Mechatronics and Machine Vision in Practice*, M2VIP 2012, 2012; p. 259-263.
20. Y. Cheng, Q. Guo, G. Tan, & P. Zhang. Improving method of image vectorization modeling for asphalt mixture. *Huazhong Keji Daxue Xuebao (Ziran Kexue Ban)*. *Journal of Huazhong University of Science and Technology (Natural Science Edition)*, 41(5), 2013; p 105-108.
21. X. Zha, L. Liu, L. Bai, & X. Han. Image recognition method of asphalt-aggregate ratio for asphalt mixture. *Jiaotong Yunshu Gongcheng Xuebao/Journal of Traffic and Transportation Engineering*, 13(1), 2013; 1-6+14.
22. H. Guler, N. Mert. A Comparative Analysis of Railway Ballast. *Proceedings of the First International Conference on Railway Technology: Research, Development and Maintenance*, J. Pombo, (Editor), Civil-Comp Press, Stirlingshire, Scotland; 2012.

23. AS 2758.7: *Aggregates and rock for engineering purposes*, Part 7: Railway ballast. Standards Australia, NSW, Australia; 1996.
24. Turkish State Railways (TCDD), *Ballast Specification, Permanent Way department*, TCDD Publications, Ankara, Turkey; 2011.
25. Italian Railways Network, RFI. *Ballast Specification RFI*, n. XXXX OD D IF SP XX.XX.X.X 001 B. 2004.

Received: 24.08.2013
Revised: 20.11.2013